



Van der Waals epitaxy of two-dimensional single-layer h-BN on graphite by molecular beam epitaxy: Electronic properties and band structure

Deborah Pierucci, Jihene Zribi, Hugo Henck, Julien Chaste, Mathieu G. Silly, François Bertran, P. Le Fevre, Bernard Gil, Alex Summerfeld, Peter Beton, et al.

► To cite this version:

Deborah Pierucci, Jihene Zribi, Hugo Henck, Julien Chaste, Mathieu G. Silly, et al.. Van der Waals epitaxy of two-dimensional single-layer h-BN on graphite by molecular beam epitaxy: Electronic properties and band structure. Applied Physics Letters, 2018, 112 (25), pp.253102. 10.1063/1.5029220 . hal-01863526

HAL Id: hal-01863526

<https://hal.science/hal-01863526>

Submitted on 3 Jun 2021



HAL is a multi-disciplinary open access archive for the deposit and dissemination of scientific research documents, whether they are published or not. The documents may come from teaching and research institutions in France or abroad, or from public or private research centers.

L'archive ouverte pluridisciplinaire **HAL**, est destinée au dépôt et à la diffusion de documents scientifiques de niveau recherche, publiés ou non, émanant des établissements d'enseignement et de recherche français ou étrangers, des laboratoires publics ou privés.

Van der Waals epitaxy of two-dimensional single-layer h-BN on graphite by molecular beam epitaxy: Electronic properties and band structure

Cite as: Appl. Phys. Lett. **112**, 253102 (2018); <https://doi.org/10.1063/1.5029220>

Submitted: 12 March 2018 . Accepted: 28 May 2018 . Published Online: 18 June 2018

Debora Pierucci, Jihene Zribi, Hugo Henck, Julien Chaste, Mathieu G. Silly,  François Bertran, Patrick Le Fevre, Bernard Gil, Alex Summerfield, Peter H. Beton,  Sergei V. Novikov, Guillaume Cassabois, Julien E. Rault, and Abdelkarim Ouerghi



View Online



Export Citation



CrossMark

ARTICLES YOU MAY BE INTERESTED IN

[High-temperature molecular beam epitaxy of hexagonal boron nitride layers](#)

Journal of Vacuum Science & Technology B **36**, 02D103 (2018); <https://doi.org/10.1116/1.5011280>

[Graphene and related two-dimensional materials: Structure-property relationships for electronics and optoelectronics](#)

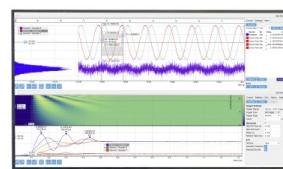
Applied Physics Reviews **4**, 021306 (2017); <https://doi.org/10.1063/1.4983646>

[Graphene-assisted quasi-van der Waals epitaxy of AlN film for ultraviolet light emitting diodes on nano-patterned sapphire substrate](#)

Applied Physics Letters **114**, 091107 (2019); <https://doi.org/10.1063/1.5081112>

Challenge us.

What are your needs for periodic signal detection?



Zurich Instruments



Van der Waals epitaxy of two-dimensional single-layer h-BN on graphite by molecular beam epitaxy: Electronic properties and band structure

Debora Pierucci,¹ Jihene Zribi,² Hugo Henck,² Julien Chaste,² Mathieu G. Silly,³ François Bertran,³ Patrick Le Fevre,³ Bernard Gil,^{4,5} Alex Summerfield,⁶ Peter H. Beton,⁶ Sergei V. Novikov,⁶ Guillaume Cassabois,⁴ Julien E. Rault,³ and Abdelkarim Ouerghi²

¹CELLS-ALBA Synchrotron Radiation Facility, Carrer de la Llum 2-26, 08290 Cerdanyola del Valles, Barcelona, Spain

²Centre de Nanosciences et de Nanotechnologies, CNRS, University Paris-Sud, Université Paris-Saclay, C2N-Marcoussis, 91460 Marcoussis, France

³Synchrotron-SOLEIL, Saint-Aubin, BP48, F91192 Gif sur Yvette Cedex, France

⁴Laboratoire Charles Coulomb UMR 5221, Université de Montpellier and CNRS, F-34095 Montpellier, France

⁵Ioffe Institute, St. Petersburg 194021, Russia

⁶School of Physics and Astronomy, University of Nottingham, Nottingham NG7 2RD, United Kingdom

(Received 12 March 2018; accepted 28 May 2018; published online 18 June 2018)

We report on the controlled growth of h-BN/graphite by means of molecular beam epitaxy. X-Ray photoelectron spectroscopy suggests the presence of an interface without any reaction or intermixing, while the angle resolved photoemission spectroscopy (ARPES) measurements show that the h-BN layers are epitaxially aligned with graphite. A well-defined band structure is revealed by ARPES measurements, reflecting the high quality of the h-BN films. The measured valence band maximum located at 2.8 eV below the Fermi level reveals the presence of undoped h-BN films (band gap ~ 6 eV). These results demonstrate that, although only weak van der Waals interactions are present between h-BN and graphite, a long range ordering of h-BN can be obtained even on polycrystalline graphite *via* van der Waals epitaxy, offering the prospect of large area, single layer h-BN. Published by AIP Publishing. <https://doi.org/10.1063/1.5029220>

Boron nitride (BN) is a synthetic material that has attracted considerable interest over the past decade.¹ BN presents four polymorphs, arising from different bonding configurations of boron (B) and nitrogen (N) atoms: cubic (c-BN), hexagonal (h-BN), rhombohedral (r-BN) and wurtzite (w-BN), and the variety of properties of BN materials are strongly related to these crystal structures. The most stable crystalline form, hexagonal h-BN, is an insulating isomorph of graphite.² The boron and nitrogen atoms are arranged in two inequivalent A and B sublattices of a planar honeycomb structure formed by sp^2 covalent bonds. As for graphite, the bonding forces between the atomic planes are of van der Waals (vdW) type. However, the band structures of h-BN and graphite show very significant differences; the different onsite energies of the B and N atoms lead to a large (~ 6 eV) band gap and a small (1.8%) lattice mismatch with graphite.^{3–6} h-BN possesses many highly desirable physical and chemical properties such as low density, high melting point, high-temperature stability, high thermal conductivity, low dielectric constant and chemical inertness.⁷ All these properties make h-BN a very interesting and unique material for various electronic and optoelectronic devices,^{8,9} either for use as a substrate or an insulating dielectric.¹⁰ With the advent of graphene and two-dimensional (2D) materials in recent years, h-BN, as the only 2D-insulator,^{11,12} is an elementary building block which may be combined with other 2D materials to form complex vdW heterostructures, thus opening a new paradigm in the physics of 2D solids.¹³ Moreover, its structural similarity to graphene and its optical properties can be utilised to improve 2D devices.^{14,15} To achieve the best possible

performance of these new 2D material vdW heterostructures, h-BN with high crystalline quality is needed.¹⁶ In semiconductor physics, it is well known that epitaxy is the most appropriate technique to obtain large area, high quality devices. However, in conventional semiconductor materials, the requirement for lattice matching limits the materials that can be combined and the quality of interfaces that can be achieved. The use of 2D materials potentially circumvents these limitations, where the relatively large lattice mismatch between different materials can be relaxed due to the weak vdW forces between 2D material layers providing virtually unlimited material combinations^{17–19} (vdW epitaxy).

We report here a combined synchrotron-based x-ray and angle-resolved photoemission spectroscopy (XPS/ARPES) study of the electronic properties and the band structure of monolayer (ML) h-BN grown on highly oriented pyrolytic graphite (HOPG) using molecular beam epitaxy (MBE). This study was also supported by micro-Raman spectroscopy and scanning electron microscopy (SEM) for morphological and elemental assessments. Despite the presence of multiple domains (causing in-plane rotational disorder) and structural defects, electronic band dispersions were clearly observed along the high symmetry direction, reflecting the high quality of h-BN films. The valence band maximum (VBM) at the K point lies 2.8 eV below the Fermi level suggesting that the h-BN layers are undoped.

Among different substrates, the use of graphite provides several potential advantages for the growth of h-BN. Figure 1(a) presents the crystal structure of the layered h-BN. Graphite and h-BN display in-plane hexagonal symmetry with lattice

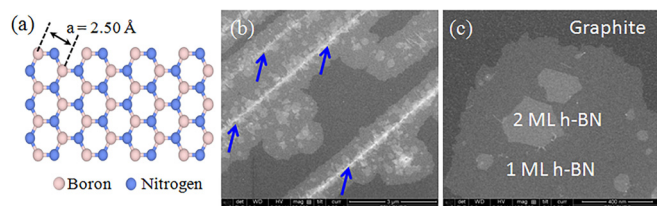


FIG. 1. (a) Crystal structure of a single layer of h-BN showing the h-BN lattice constant. (b) SEM image of h-BN growth on HOPG showing nucleation from HOPG in terrace steps indicated by the blue arrows. The darker contrast region corresponds to the underlying HOPG substrate and the lighter regions correspond to regions of h-BN growth. (c) High resolution SEM image of an h-BN island showing regions of single and bi-layer growth and a region of exposed HOPG substrate.

constants of $a_{\text{h-BN}} = 0.250 \text{ nm}$ and $a_{\text{Graphite}} = 0.246 \text{ nm}$, making them highly compatible materials. Single layer h-BN was grown on HOPG using high-temperature MBE as described previously.^{20,21} The graphite substrate is a very inert surface ensuring the presence of only vdW interactions between h-BN and the substrate.²² Figures 1(b) and 1(c) show SEM images for a growth temperature of 1480°C . Bright lines [indicated by the blue arrows in Fig. 1(b)] are observed using SEM which correspond to the positions of the graphite step edges and indicate that the h-BN primarily nucleates from these regions. The h-BN ribbons form a partial single layer along with very small multi-layer regions (bilayer or trilayer h-BN) as shown in Fig. 1(c). The ribbons are $\sim 1 \mu\text{m}$ wide and $\sim 50 \mu\text{m}$ long and are in agreement with our previous observations of h-BN grown on HOPG under similar conditions.^{21,23} It is worthwhile noting that some of these ribbons are much wider than the underlying step distances on the substrate ($\sim 500 \text{ nm}$), suggesting that h-BN then grows laterally across the terrace before coalescing to form a uniform layer. The lateral growth of h-BN is confirmed by Fig. 1(c), which displays large h-BN monolayers, suggesting that the domains grow partially from secondary nucleation events, although we cannot exclude the formation of a domain boundary on a low scale resulting from the coalescence of different h-BN domains as reported in similar studies using atomic force microscopy.²⁰

Using high resolution X-ray photoelectron spectroscopy (HR-XPS), we investigated the atomic composition as well as the chemical bonding environment of our samples. The XPS measurements (Fig. S2) performed over a wide energy range ($h\nu = 825 \text{ eV}$) showed that only a small amount of oxygen contamination is present in the sample after the annealing process. The growth of the h-BN monolayer on the HOPG substrate was confirmed by the presence of B 1s and N 1s core level peaks. High resolution spectra are shown in Figs. 2(a)–2(c). The experimental data points are displayed as dots. The solid line is the envelope of the fitted components. The underlying HOPG gives rise to a unique narrow (FWHM = 0.8 eV) carbon C 1s [binding energy (BE) = 284.4 eV] peak which presents a characteristic dissymmetric shape, i.e., broadening on its high energy side. This shape is expected for a conductive material and well described using a Doniach-Sunjić fitting curve considering an asymmetry value $\alpha = 0.14$.²⁴ In addition to this main peak, an inter-band π - π^* transition peak is present at higher binding energies (about 6 eV shift).²⁴ Also, one main sharp

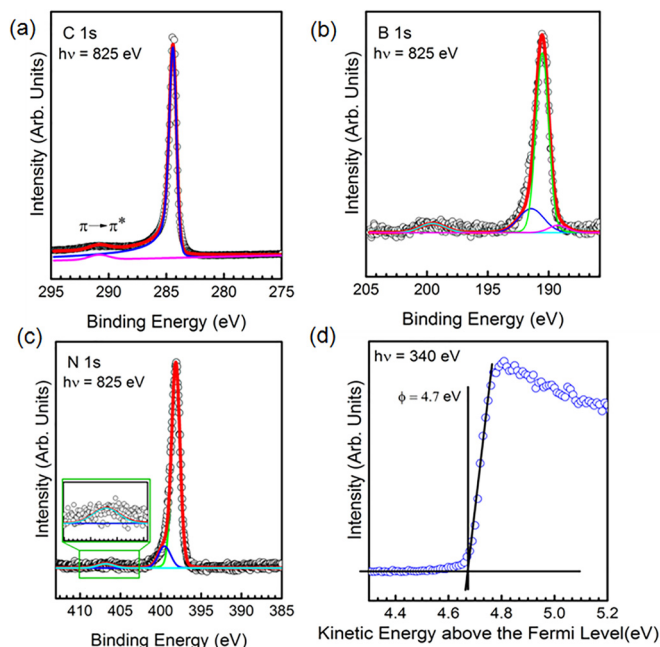


FIG. 2. HR-XPS spectra of (a) carbon 1s (b) boron 1s and (c) nitrogen 1s peaks (insert: a zoom-in view of the π plasmon), respectively, measured at $h\nu = 825 \text{ eV}$. (d) Secondary electron intensity as a function of the kinetic energy above the Fermi level for the h-BN/graphite heterostructure measured at $h\nu = 340 \text{ eV}$.

peak (FWHM $\sim 1.2 \text{ eV}$) is observed in the B 1s and N 1s spectra at BEs of 190.5 eV and 398.1 eV , respectively. Overall, these results suggest a main chemical environment corresponding to the B-N bond in the hexagonal structure present in an h-BN layer.^{25–30} The hexagonal structure of the BN sample is confirmed by the presence in both spectra of a peak at a higher binding energy ($\sim 9 \text{ eV}$) than the main peak, which corresponds to a π plasmon (in light blue color). This loss feature is present only in hexagonal BN as there are no π electrons in cubic BN.³¹

The presence of grain boundaries in the sample can be related to the presence of defects and preferential sites for adsorbates (e.g., oxygen). Recent works^{32,33} have shown that in the case of h-BN, the grain boundaries are mostly formed by the pentagon-heptagon (5–7) ring fusion which introduces homo-elemental bonding (either B-B or N-N). The presence of these two types of defects is clearly visible in the HR-XPS deconvolution of the B 1s and N 1s spectra. At first, a small shoulder located at $+0.9 \text{ eV}$, with respect to the main peak, is present in the B 1s spectrum. This component, representing 17% of the total photoemission intensity, can be attributed to a nitrogen vacancy which is replaced by an oxygen atom forming a B-O bond.^{22,34} In the B 1s spectrum, another small component is present at a lower binding energy than the main peak (-1.3 eV). This peak, as the one located at $+1.4 \text{ eV}$ in the N 1s spectrum, is the signature of a 5–7 ring attributed to the presence of grain boundaries. In particular, these features indicate the formation of homo-nuclear bonds B-B and N-N, respectively.^{34–36} No other components are present in the B 1s and N 1s spectra at lower binding energies, indicative of B-C^{37,38} or N-C^{37,38} or at higher energies, indicating N-O^{22,38,39} bonds. Therefore, besides the presence of grain boundaries and nitrogen vacancies, induced naturally by the island conformation of the h-BN flakes, the

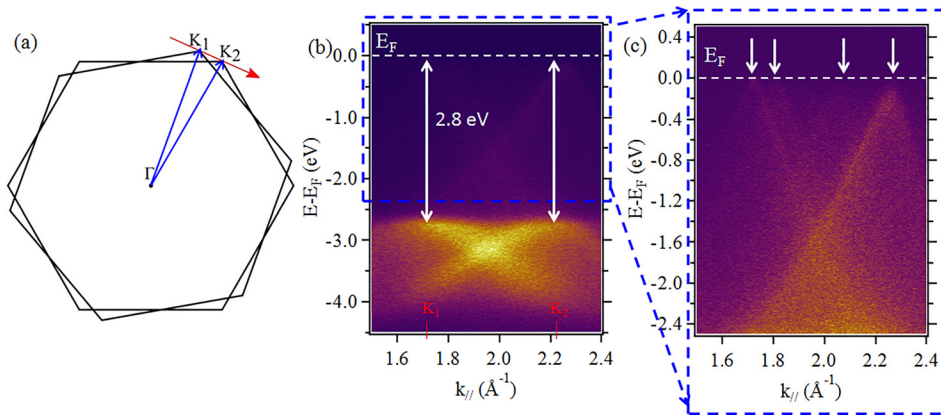


FIG. 3. (a) h-BN Brillouin zone as seen in the ARPES map of (b) due to two h-BN domains. K_1 and K_2 indicate the K point relative to these domains. The red arrow represents the measurement geometry in k -space. (b) ARPES measurements of h-BN and (c) a zoom-in view of ARPES measurements in (b) showing the band structure of the graphite substrate capped with h-BN at $h\nu = 60$ eV and 8 K. The white arrows point to different K points related to different graphite domains. The Fermi level position is located at zero binding energy [indicated by the white dashed line in both (b) and (c)].

sample shows high crystalline quality. In fact, the comparison of these HR-XPS spectra with our previous study carried out on a bulk h-BN flake⁴⁰ shows that the FWHM of the main XPS components is of the same order of magnitude (1 eV for the bulk h-BN and 1.2 eV in the case of polycrystalline single layer h-BN). The measurement of the secondary electron cut off [Fig. 2(d)] allows the determination of the work function (ϕ) of our h-BN flakes grown on the HOPG substrate, $\phi_{h\text{-BN}/\text{HOPG}} = 4.70 \pm 0.05$ eV. This value is really sensitive to the h-BN substrate and the type of interface bonding.^{41–43}

This high degree of crystalline order is also confirmed by the NEXAFS analysis (Sec. S3, [supplementary material](#)). The angle-dependent NEXAFS spectra at the nitrogen K-edge [Fig. S3(a)] and at the B K-edge [Fig. S3(b)] show a strong dichroism of the π^* and σ^* resonances, clearly indicating that the h-BN layers grow parallel to the graphite substrate. In order to gain an insight into the strength of the interaction between h-BN and graphite and determine the electronic properties of h-BN, ARPES was used to measure the band structure of single layer h-BN on graphite.^{40,44} The ARPES intensity map was measured perpendicular to the ΓK direction of the h-BN Brillouin zone [Fig. 3(a)] in order to discriminate between different h-BN and graphite domain orientations. Figure 3(b) shows the dispersion of the h-BN bands measured on the graphite substrate. The lower intensity bands between -2 eV and E_F are due to the π bands of graphite domains [Fig. 3(c)]. The figure shows two bright and one faint intersecting Dirac cones. These arise from different graphite domains within the HOPG surface; the difference in their relative orientation is reflected in different in-plane wave-vectors on which they are centered (white arrows). Note that the spot size used for the ARPES measurements is ~ 50 μm , which is sufficient to illuminate an area on the surface containing more than one HOPG domain. Band maps on different areas of the sample show similar features: multiple rotated linearly dispersing Dirac cones. The h-BN VBM overlaps with the π graphite bands, but can be seen to be ~ 2.8 eV below the Fermi level consistent with a 6 eV band gap and similar to that found for single layer h-BN.⁶ The high intensity and sharpness of the π bands attest the high quality of the h-BN sample. The presence of a single π band is a clear signature of the single layer h-BN band structure.⁴⁵ This is confirmed by the location of this VBM at the K point, in contrast to multilayer h-BN.⁴⁰ Similar to the

HOPG substrate, we find domains of h-BN with different orientations suggesting the presence of rotational disorder and twinning domains. However, there is a local match of the alignment between h-BN and graphite; that is, the valence band maximum of each h-BN domain occurs at the same in-plane vector as the Dirac point of graphite implying that lattice vectors of h-BN and graphite are locally orientationally aligned. Based on the difference in the wave vector between the two domains, we can estimate the rotation angle of the particular areas which contribute to the measurements in Fig. 3, and the angle is estimated to be about 10° . These results indicate that, despite a weak interaction between h-BN and graphite, van der Waals epitaxy defines the long range ordering of h-BN, even on graphite. Note that AFM images published previously have identified small h-BN domains which grow with different orientational alignments.^{18,19} The results present here show that when averaged over large areas, orientational alignment does occur, suggesting possibly that islands with orientational alignment grow more rapidly than misaligned islands. On the basis of these ARPES and HR-XPS measurements, the band alignment of the h-BN/HOPG system (Fig. 4) was also determined. This band alignment is expected to differ for the case of 3D materials junction. In fact, the low dimensionality of 1 ML h-BN (few \AA thick) prohibits the formation of a depletion region. This region is replaced by what is called a van der Waals gap, as shown in Fig. 4. Moreover, the lack of dangling bonds on both surfaces (HOPG and h-BN) implies the absence of surface states (no Fermi level pinning); no bonds are present at the interface between the two materials (as confirmed also by XPS measurements Fig. 2), which are held together only by vdW

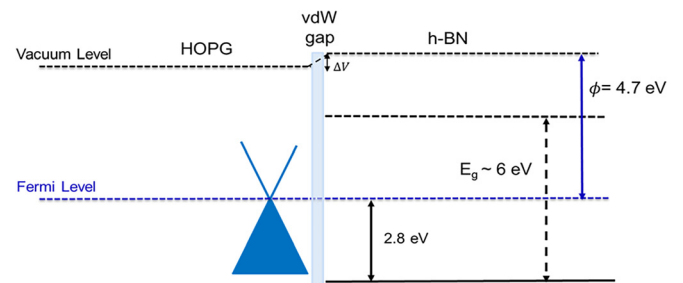


FIG. 4. Band alignment diagram of h-BN/graphite obtained from ARPES and HR-XPS measurements. The h-BN VBM is located at -2.8 eV with respect to the Fermi level and the work function of the system is 4.7 eV. A small dipole is present at the interface $\Delta V = 0.1$ eV.

interaction. Then, the band alignment is governed by the Schottky-Mott limit (S parameter close to 1).^{46–48} However, although vdW interaction is weak, it can redistribute the charge density at the interface that can induce an interface dipole⁴⁹ $\Delta V = \phi_{h\text{-BN/HOPG}} - \phi_{\text{HOPG}} = 4.7 - 4.6 = 0.1$ eV (Ref. 50). These results show the formation of a vdW heterostructure where the MBE grown h-BN is un-doped and electronically decoupled from the surface, maintaining its insulating character.

In summary, we have studied the electronic properties and the band structure of single layer h-BN grown on graphite using MBE. We find that this heterostructure gives rise to sharp bands, in particular for the h-BN valence bands at the K points. Our ARPES measurements of the heterostructure showed that graphite and h-BN largely retain their original electronic structure. The obtained epitaxial films of single layer h-BN demonstrate very high structural perfection as confirmed using HR-XPS and NEXAFS. ARPES experiments demonstrate clearly the energy dispersion of the valence band of single layer h-BN below the Fermi level. The h-BN layer is electronically decoupled from the graphite surface, as expected in van der Waals epitaxy of a layered material such as h-BN.

See [supplementary material](#) for Methods and characterization, Fig. S1: Raman spectroscopy study of a h-BN/graphite sample. Figure S2: A wide energy range HR-XPS spectrum of h-BN/HOPG collected at a photon energy $h\nu = 825$ eV. Figure S3: Partial yield absorption of (a) nitrogen and (b) boron K-edge NEXAFS spectra as a function of the angle between the polarization vector \vec{E} and the surface normal \vec{n} (θ).

This work was supported by the H2DH and RhomboG Grants. We acknowledge support from GANEX (Grant No. ANR-11-LABX-0014) and Labex “Nanosaclay (Grant No. ANR-10-LABX-0035)”. GANEX belongs to the public funded “Investissements d’Avenir” program managed by the French National Research Agency. This work was partly supported by the Government of the Russian Federation (Contract No. 14.W03.31.0011 at the IOFFE Institute of RAS). This work was supported by the Engineering and Physical Sciences Research Council [Grant numbers EP/L013908/1, EP/P019080/1 and EP/M50810X/1]; and by the Leverhulme Trust [Grant number RPG-2014-129]. P.H.B. and S.V.N. acknowledge the help of Dr. T. S. Cheng, Dr. Y. J. Cho, Dr. E. F. Smith, and Dr. C. J. Mellor.

¹K. Watanabe, T. Taniguchi, and H. Kanda, *Nat. Mater.* **3**, 404 (2004).

²K. H. Lee, H.-J. Shin, J. Lee, I. Lee, G.-H. Kim, J.-Y. Choi, and S.-W. Kim, *Nano Lett.* **12**, 714 (2012).

³G. Fugallo, M. Aramini, J. Koskelo, K. Watanabe, T. Taniguchi, M. Hakala, S. Huotari, M. Gatti, and F. Sottile, *Phys. Rev. B* **92**, 165122 (2015).

⁴L. Ju, J. Velasco, E. Huang, S. Kahn, C. Nosioglia, H.-Z. Tsai, W. Yang, T. Taniguchi, K. Watanabe, Y. Zhang, G. Zhang, M. Crommie, a Zettl, and F. Wang, *Nat. Nanotechnol.* **9**, 348 (2014).

⁵T. Galvani, F. Paleari, H. P. C. Miranda, A. Molina-Sánchez, L. Wirtz, S. Latil, H. Amara, and F. Ducastelle, *Phys. Rev. B* **94**, 125303 (2016).

⁶G. Cassabo, P. Valvin, and B. Gil, *Nat. Photonics* **10**, 262 (2016).

⁷L. Liu, Y. Feng, and Z. Shen, *Phys. Rev. B* **68**, 104102 (2003).

⁸L. Britnell, R. V. Gorbachev, R. Jalil, B. D. Belle, F. Schedin, M. I. Katsnelson, L. Eaves, S. V. Morozov, A. S. Mayorov, N. M. R. Peres,

A. H. C. Neto, J. Leist, A. K. Geim, L. A. Ponomarenko, and K. S. Novoselov, *Nano Lett.* **12**, 1707 (2012).

⁹Z. Liu, L. Ma, G. Shi, W. Zhou, Y. Gong, S. Lei, X. Yang, J. Zhang, J. Yu, K. P. Hackenberg, A. Babakhani, J.-C. Idrobo, R. Vajtai, J. Lou, and P. M. Ajayan, *Nat. Nanotechnol.* **8**, 119 (2013).

¹⁰L. Sponza, H. Amara, F. Ducastelle, A. Loiseau, and C. Attaccalite, *Phys. Rev. B* **97**, 075121 (2018).

¹¹T. Q. P. Vuong, G. Cassabo, P. Valvin, A. Ouerghi, Y. Chassagneux, C. Voisin, and B. Gil, *Phys. Rev. Lett.* **117**, 097402 (2016).

¹²G. Cassabo, P. Valvin, and B. Gil, *Phys. Rev. B* **93**, 035207 (2016).

¹³A. K. Geim and I. V. Grigorieva, *Nature* **499**, 419 (2013).

¹⁴C. R. Dean, A. F. Young, I. Meric, C. Lee, L. Wang, S. Sorgenfrei, K. Watanabe, T. Taniguchi, P. Kim, K. L. Shepard, and J. Hone, *Nat. Nanotechnol.* **5**, 722 (2010).

¹⁵G.-H. Lee, Y.-J. Yu, C. Lee, C. Dean, K. L. Shepard, P. Kim, and J. Hone, *Appl. Phys. Lett.* **99**, 243114 (2011).

¹⁶P. Sutter, R. Cortes, J. Lahiri, and E. Sutter, *Nano Lett.* **12**, 4869 (2012).

¹⁷A. Koma, *J. Cryst. Growth* **201–202**, 236 (1999).

¹⁸Z. Ben Aziza, D. Pierucci, H. Henck, M. G. Silly, C. David, M. Yoon, F. Sirotti, K. Xiao, M. Eddrief, J. Girard, and A. Ouerghi, *Phys. Rev. B* **96**, 035407 (2017).

¹⁹Z. Ben Aziza, H. Henck, D. Pierucci, M. G. Silly, E. Lhuillier, G. Patriarche, F. Sirotti, M. Eddrief, and A. Ouerghi, *ACS Nano* **10**, 9679 (2016).

²⁰Y.-J. Cho, A. Summerfield, A. Davies, T. S. Cheng, E. F. Smith, C. J. Mellor, A. N. Khlobystov, C. T. Foxon, L. Eaves, P. H. Beton, and S. V. Novikov, *Sci. Rep.* **6**, 34474 (2016).

²¹T. Q. P. Vuong, G. Cassabo, P. Valvin, E. Rousseau, A. Summerfield, C. J. Mellor, Y. J. Cho, T. S. Cheng, J. D. Albar, L. Eaves, C. T. Foxon, P. H. Beton, S. V. Novikov, and B. Gil, *2D Mater.* **4**, 21023 (2017).

²²H. Sediri, D. Pierucci, M. Hajlaoui, H. Henck, G. Patriarche, Y. J. Dappe, S. Yuan, B. Toury, R. Belkhou, M. G. Silly, F. Sirotti, M. Boutchich, and A. Ouerghi, *Sci. Rep.* **5**, 16465 (2015).

²³T. S. Cheng, A. Summerfield, C. J. Mellor, A. Davies, A. N. Khlobystov, L. Eaves, C. T. Foxon, P. H. Beton, and S. V. Novikov, *J. Vac. Sci. Technol. B* **36**, 02D103 (2018).

²⁴P. M. T. M. Van Attekum and G. K. Wertheim, *Phys. Rev. Lett.* **43**, 1896 (1979).

²⁵Q. Wu, J.-H. Park, S. Park, S. J. Jung, H. Suh, N. Park, W. Wongwiriyan, S. Lee, Y. H. Lee, and Y. J. Song, *Sci. Rep.* **5**, 16159 (2015).

²⁶M. C. Polo, E. Martinez, J. Esteve, and J. L. Andújar, *Diamond Relat. Mater.* **7**, 376 (1998).

²⁷K. S. Park, D. Y. Lee, K. J. Kim, and D. W. Moon, *Appl. Phys. Lett.* **70**, 315 (1997).

²⁸W. Lei, D. Portehault, R. Dimova, and M. Antonietti, *J. Am. Chem. Soc.* **133**, 7121 (2011).

²⁹R. Sevak Singh, R. Yingjie Tay, W. Leong Chow, S. Hon Tsang, G. Mallick, and E. H. Tong Teo, *Appl. Phys. Lett.* **104**, 163101 (2014).

³⁰Z. Liu, L. Song, S. Zhao, J. Huang, L. Ma, J. Zhang, J. Lou, and P. M. Ajayan, *Nano Lett.* **11**, 2032 (2011).

³¹R. Trehan, Y. Lifshitz, and J. W. Rabalais, *J. Vac. Sci. Technol. A: Vac., Surf., Films* **8**, 4026 (1990).

³²A. L. Gibb, N. Alem, J. H. Chen, K. J. Erickson, J. Ciston, A. Gautam, M. Linck, and A. Zettl, *J. Am. Chem. Soc.* **135**, 6758 (2013).

³³Y. Liu, X. Zou, and B. I. Yakobson, *ACS Nano* **6**, 7053 (2012).

³⁴W. Orellana and H. Chacham, *Phys. Rev. B* **63**, 125205 (2001).

³⁵M. F. Genisel, M. N. Uddin, Z. Say, M. Kulakci, R. Turan, O. Gulseren, and E. Bengu, *J. Appl. Phys.* **110**, 074906 (2011).

³⁶L. Guo, R. N. Singh, and H. J. Kleebe, *J. Nanomater.* **2006**, 1 (2006).

³⁷T. SUGINO and T. TAI, *Jpn. J. Appl. Phys., Part 2* **39**, L1101 (2000).

³⁸T. Sugino, T. Tai, and Y. Etou, *Diamond Relat. Mater.* **10**, 1375 (2001).

³⁹W. J. Pan, J. Sun, H. Ling, N. Xu, Z. F. Ying, and J. D. Wu, *Appl. Surf. Sci.* **218**, 298 (2003).

⁴⁰H. Henck, D. Pierucci, G. Fugallo, J. Avila, G. Cassabo, Y. J. Dappe, M. G. Silly, C. Chen, B. Gil, M. Gatti, F. Sottile, F. Sirotti, M. C. Asensio, and A. Ouerghi, *Phys. Rev. B* **95**, 85410 (2017).

⁴¹M. Bokdam, G. Brocks, M. I. Katsnelson, and P. J. Kelly, *Phys. Rev. B* **90**, 85415 (2014).

⁴²F. Schulz, R. Drost, S. K. Hämäläinen, T. Demonchaux, A. P. Seitsonen, and P. Liljeroth, *Phys. Rev. B* **89**, 235429 (2014).

⁴³S. Joshi, D. Ecija, R. Koitz, M. Iannuzzi, A. P. Seitsonen, J. Hutter, H. Sachdev, S. Vijayaraghavan, F. Bischoff, K. Seufert, J. V. Barth, and W. Auwärter, *Nano Lett.* **12**, 5821 (2012).

⁴⁴H. Henck, D. Pierucci, Z. Ben Aziza, M. G. Silly, B. Gil, F. Sirotti, G. Cassabo, and A. Ouerghi, *Appl. Phys. Lett.* **110**, 23101 (2017).

- ⁴⁵D. Usachov, V. K. Adamchuk, D. Haberer, a Grüneis, H. Sachdev, a. B. Preobrajenski, C. Laubschat, and D. V. Vyalikh, [Phys. Rev. B](#) **82**, 75415 (2010).
- ⁴⁶R. T. Tung, [Appl. Phys. Rev.](#) **1**, 011304 (2014).
- ⁴⁷T. Le Quang, V. Cherkov, K. Nogajewski, M. Potemski, M. T. Dau, M. Jamet, P. Mallet, and J.-Y. Veuillen, [2D Mater.](#) **4**, 35019 (2017).
- ⁴⁸D. Pierucci, H. Henck, J. Avila, A. Balan, C. H. Naylor, G. Patriarche, Y. J. Dappe, M. G. Silly, F. Sirotti, A. T. C. Johnson, M. C. Asensio, and A. Ouerghi, [Nano Lett.](#) **16**, 4054 (2016).
- ⁴⁹C. Si, Z. Lin, J. Zhou, and Z. Sun, [2D Mater.](#) **4**, 15027 (2016).
- ⁵⁰H. Hibino, H. Kageshima, M. Kotsugi, F. Maeda, F.-Z. Guo, and Y. Watanabe, [Phys. Rev. B](#) **79**, 125437 (2009).